Chemical Engineering Science 243 (2021) 116732

Contents lists available at ScienceDirect

Chemical Engineering Science

journal homepage: www.elsevier.com/locate/ces

Effect of solid loading and particle size on the phase holdup distribution and bubble behaviour in a pilot-scale slurry bubble column

Mojtaba Mokhtari, Jamal Chaouki *

Department of Chemical Engineering, Ecole Polytechnique de Montreal, Montreal, QC, Canada

HIGHLIGHTS

- New phenomenological model was developed to predict solids distribution.
- Optical fiber probes are used for simultaneous measuring of the solids and gas holdups.
- Effect of particle size on the shape of radial solids distribution was negligible.
- The initial bubble size was independent of the particle size.
- Small particles lead to more bubble coalescence.

ARTICLE INFO

Article history:
Received 3 December 2020
Received in revised form 23 February 2021
Accepted 30 April 2021
Available online 20 May 2021

Keywords:
Bubble column
Radial solids holdup
Gas holdup
Optical fiber probe
Particle size

ABSTRACT

Complexities in the hydrodynamics of slurry bubble columns lead to noticeable uncertainty in the design and scale-up of these multiphase reactors. Knowledge of local hydrodynamics can alleviate this problem. The effect of solids properties on the local hydrodynamic parameters is a critical subject where the lack of knowledge is undeniable. In the present study, optical fiber probes were used to study the effect of particle size and concentration on the solids and gas distribution inside the bubble column. A pilot-scale cylindrical bubble column 270 cm in height and 29.2 cm in diameter was employed. Glass beads with various mean diameters (35, 71, 156 μm) and 1, 3 and 5 vol% were added to tap water in order to make the slurry phase. Air with a wide range of superficial gas velocities (up to 20 cm/s) was injected into the slurry phase. The results demonstrated that the solid particles' radial and axial distributions were not uniform in the column. Solids concentration showed a local maximum in the near-wall region. Gas holdup had a parabolic shape except for large particles at high solids concentration in which the maximum of the gas holdup was observed at the sides rather than the centerline. The variations in the pressure fluctuations revealed that the particle size decrease led to an increase in the bubble size; however, the initial bubble size was independent of the particle size. Moreover, the increase in the solids concentration resulted in an increase in the gas holdup in the homogeneous flow regime; and a decrease in the heterogeneous one. Finally, a predictive model that can estimate the radial and axial solids distributions in the slurry bubble column is presented.

1. Introduction

Slurry bubble column reactors (SBCR) have many essential advantages in comparison to other multiphase reactors. The construction of a SBCR, for instance, is quite simple. SBCRs also provide relatively high heat and mass transfer rates in addition to the capability of working with small solid catalysts. Consequently, many processes in the chemical, petrochemical and bio industries opt for the slurry bubble column as an efficient way to produce their desired products. Despite these advantages, the design and scale-up of SBCRs are problematic due to the complexity of the hydrodynamics.

Much research has been done to better understand the hydrodynamic parameters of the bubble column (Shu et al., 2019). The majority focused on the two-phase systems; however, solid particles, as a catalyst or reactant, are commonly applied in industrial applications of the bubble column. The presence of solid particles leads to a substantial difference in hydrodynamics. Some researchers tried to investigate the solid's effect on the gas holdup, bubble behaviour, and the liquid flow pattern (An et al., 2020; Rabha et al., 2013; Gheni et al., 2016; Prakash et al., 2019; Sarhana et al.,

* Corresponding author.
E-mail address: jamal.chaouki@polymtl.ca (J. Chaouki).

https://doi.org/10.1016/j.ces.2021.116732
0009-2509/

Nomenclatures

C	Solids concentration (kg/m^3)
C_0	Overall solids concentration (kg/m^3)
C_V	Solids volume/Volume Fraction in the slurry phase (-)
D_s	Mass diffusivity of the solid phase (m^2/s)
D	Column diameter (m)
K	A constant in Eq (8). (kg/m^3)
L	Bed height (m)
L_0	Initial (unaerated) bed height (m)
m	Mass (kg)
$\dot{m}$	Mass flux (kg/m^2/s)
N	Number of data points, a constant in Eq (4).
n	A constant in Eq (7).
R	Column radius (m)
r	Position in the radial direction (m)
t	Time (s)
U_G	Superficial gas velocity (cm/s)
V	Volume (m^3), Velocity (m/s)
V_0	Axial velocity of the slurry at centerline (m/s)
V_p	Slip velocity of the particle (m/s)
Vt	Terminal Velocity of a single particle (m/s)
ΔP	The pressure difference (pa)
Z	Distance in elevation (m)
P	Pressure (pa)
Pe	Peclet number (-)
ε	Phase holdup (-)
ε_g	Overall gas holdup (-)
μ	The average pressure in the pressure fluctuations
σ	The Standard deviation of the pressure
ρ	Density (kg/m^3)
ξ	Slip Ratio (-)
θ	Angular Position (radians)

Subscripts

G	Gas phase
r	Radial direction
L	Liquid phase
S	Solid Phase
SL	Slurry
Res	Residence
z	Axial direction

2018; Zhou et al., 2020). Nevertheless, the number of studies focusing on the effect of particle properties on local hydrodynamics remained low.

Due to the undeniable influence of solids distribution on the performance of SBCRs, researchers have tried to measure the local solids holdup in slurry bubble columns (Warsito et al., 1999; Soong et al., 2000; Jin et al., 2010; Sines et al., 2019; Rados et al., 2005; Abdullah, 2019; Mokhtari and Chaouki, 2019). There are, however, limitations in the measurement techniques. Ultrasonic (Warsito et al., 1999; Soong et al., 2000), Electrical Resistance Tomography (ERT) (Jin et al., 2010; Sines et al., 2019), gamma-ray computed tomography (GRCT) (Rados et al., 2005), and a sampling technique (Abdullah, 2019) have been used to measure the local solids concentration in slurry bubble columns. These techniques are neither sufficiently accurate nor suitable for various process situations. For instance, the ultrasonic technique can be used in low solid and gas holdup, and the ERT and single-source GRCT indirectly measure the solid holdup using the gas holdup from another technique. Recently, Mokhtari and Chaouki (2019) developed a new measurement technique by applying optical fiber probes. An OFP has the advantage of directly measuring the local solids concentration and gas holdup simultaneously. This method was adopted in the present study.

The effect of particle size and concentration on bubble behaviour and gas holdup distribution is another issue that requires more investigation (Orvalho et al., 2018). It is believed that the presence of the hydrophilic particles in the system leads to a decrease in the gas holdup, as they can raise the bubble coalescence rate; Consequently, the average bubble size increase, which leads to a reduction in the overall gas holdup.

The reported results on the particle size's role are contradictory, and both increases and decreases in the gas holdup can be found in the literature. Lakhdissi et al. (2020) observed that the gas holdup decreases with an increase in the particle size. They adopted glass beads in the range of 35 to 156 μm and measured the gas holdups by differential pressure transducers. Moreover, Rabha et al. (2013) claimed that the averaged bubble size increases with an increase in particle size, which leads to a decrease in the overall gas holdup.

In contrast, Sarhana et al. (2018) observed a decrease in bubble coalescence and bubble size due to an increase in particle size. Consequently, the gas holdup increased. Also, Kim et al. (1987) showed that the gas holdup increases by increments of the particle diameter while the particles are smaller than 200 μm. It is ascribed to the decrease in the apparent viscosity by increasing particle diameter, leading to a decrease in the bubble size. It can also be attributed to the particle-bubble collisions, which may reduce the bubble velocity (Lakhdissi et al., 2020). Large particles have a high collision efficiency; therefore, they show a noticeable impact on the bubble velocity, resulting in gas holdup increments.

Current information about the particle size's influence on gas holdup and bubble size is insufficient, which is motivation enough to investigate more and improve our knowledge in this area. In the present study, the particle size's effect on the local distribution of the solids and gas holdups is investigated. Optical fiber probes were employed to measure the solids and gas holdup simultaneously. Absolute pressure transducers were used to observe the particles' influence on the bubble size, qualitatively. In addition, a phenomenological model was developed to predict the radial and axial solids distribution inside the SBCRs.

2. Experimental procedure

2.1. Bubble column and materials

A plexiglass column with a 29.2 cm diameter and a height of 270 cm was used as the pilot-scale bubble column in the present work. A perforated plate was employed as the gas distributor. The plate contains 94 holes (density of 1400 holes/m^2) with a 1 mm diameter. The volumetric air flow rate was measured by two rotameters, capable of adjusting the superficial gas velocity from 0.5 cm/s up to 20 cm/s. Therefore, the slurry bubble column can operate in the homogeneous and also heterogeneous flow regime. The slurry phase's initial level was 110 cm, and its superficial velocity was zero in all experiments.

Three different sizes of glass bead particles were adopted as the solid phase to define the particle size's effect on the hydrodynamic parameters. Also, various solid loading (1,3 and 5 vol%) for each particle was chosen to evaluate the solids loading influence. The following table shows the properties of the particles.

Fig. 1 shows a schematic of the bubble column and the position of the optical fiber probes and the pressure transducers, which were applied as measurement devices.

2.2. Measurement techniques

Three absolute pressure transducers (OMEGA PX-429) were employed to measure the local pressure fluctuation in the bottom, middle and top of the column to estimate the variations in bubble size. The radial and axial distribution of the solids and gas holdup were measured by in-house made optical fiber probes.

2.2.1. Absolute pressure transducer

The pressure fluctuations, which are obtained from the absolute pressure transducers, are analyzed based on the signal amplitude and the Standard deviation of the signals (Esmaeili et al., 2015). The Standard deviation (SD) for N data is calculated by:

$$\sigma = \sqrt{\frac{1}{N-1}\sum_{n=1}^{N}(P_n - \mu)^2}$$

In which μ is the average and equal to,

$$\mu = \frac{1}{N}\sum_{n=1}^{N} P_n$$

As generally known, the standard deviation is an index of the dataset dispersion from its mean value. The passage of bubbles causes pressure to diverge from its steady value. The pressure fluctuations increase due to an increase in bubble size as a larger bubble has more influence on the surrounding area (Ruthiya et al., 2005). So, the SD increase relates to the rise in the number of large bubbles and/or the size of the bubbles. Consequently, the standard deviation is an index to evaluate the bubble size. To be able to compare the standard deviations of the different data sets, it is better to use the standard deviation ratio, which is σ/μ.

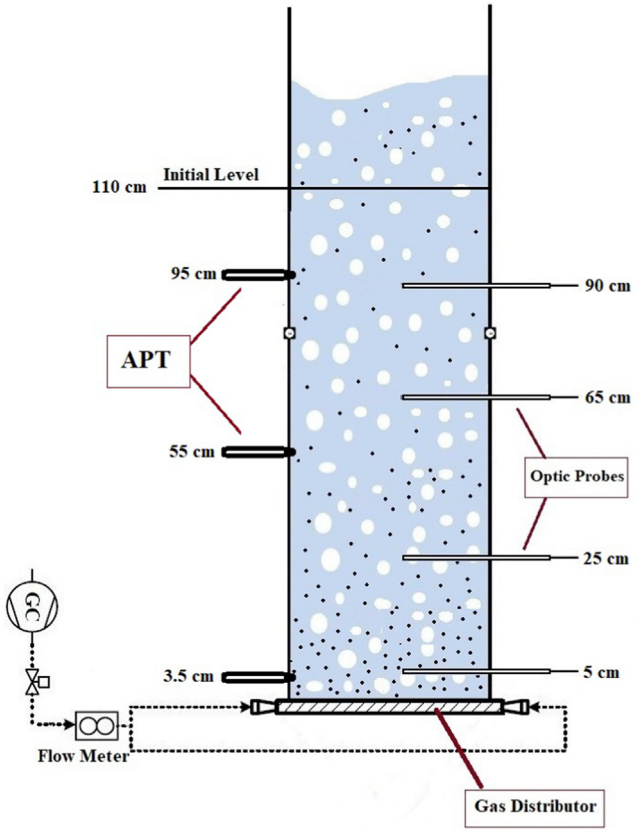

Fig. 1. Schematic view of the Bubble column.

2.2.2. Optical fiber probe

Various researchers adopted different types of optical fiber probes (OFP) to measure bubble characteristics (Besagni and Inzoli, 2016; Wang et al., 2017; Manjrekar and Dudukovic, 2015; Esmaeili et al., 2015; Hernandez-Alvarado et al., 2018). This measurement device is commonly used to measure the local gas holdup, bubble size and bubble rise velocity. In the present study, in-house made probes were employed to measure both local gas and solid holdup. The probes have one tip, which is 3 mm in diameter and consists of 72 plastic optical fiber strings that emit and receive light. The probes are horizontally placed in the slurry bubble column. Visible light generated by a light source is sent to the column by the probe. A specific amount of light is reflected by the medium and returns to the probe's tip. The reflected light is converted to voltage by photoelectric multipliers. Subsequently, a data acquisition system is applied to record the voltage signals.

As already mentioned, the amount of reflected light and, consequently, the intensity of the recorded voltage depend on the refractive index of the medium. A peak is observed when the tip of the probe is inside a bubble. So, the peaks in the signals are related to the gas phase. By interpreting these signals, the gas holdup is calculated by (Mokhtari and Chaouki, 2019):

$$\varepsilon_{g,local} = \frac{\sum_{i=1}^{n} t_{res}(i)}{t}$$

In which the t_{res} is the time that each bubble takes to pass the tip of the probe. The summation of these times for all measured bubbles (n = number of bubbles) per total measurement time is the gas holdup.

In addition, the intensity of the reflected light from the slurry phase changes due to variation in the slurry phase's properties. So, it is possible to measure the solids concentration using a calibration that relates the solids concentration to the recorded voltage

A two-phase continuous stirred tank was used to obtain a calibration curve. It was observed that the solid–liquid system can reach a uniform mixture in the tank (Mokhtari and Chaouki, 2019). Therefore, the solids concentration which matches the recorded voltage will be,

$$C_V = \frac{V_S}{V_{Total}} = \frac{m_{s/\rho_S}}{V_L + m_{s/\rho_S}}$$

Finally, a calibration curve can be obtained by changing the x and recording the voltage. More details about the calibration methodology and the measurement of the solids concentration in the slurry bubble column were published elsewhere (Mokhtari and Chaouki, 2019). Fig. 2 shows the calibration curves. The experiments in the calibration process were repeated three times to ensure the reliability of the calibrations. The average of uncertainties was less than 5 percent (standard deviation). The amount of the voltage is profoundly affected by the particle size. At the same concentration, large particles reflect less light due to the lower total surface area they have (the number of large particles in the same concentration is very low compared to the small particles). So, segregation could be a challenge for measurement. Suppose that segregation occurs in the bubble column. In this case, the OFP cannot be used because it is impossible to define if the probe's voltage changes due to the variation of concentration or particle size. A sampling technique was performed to examine the segregation in the slurry bubble column. The samples were taken from various positions of the column. A particle size analyzer

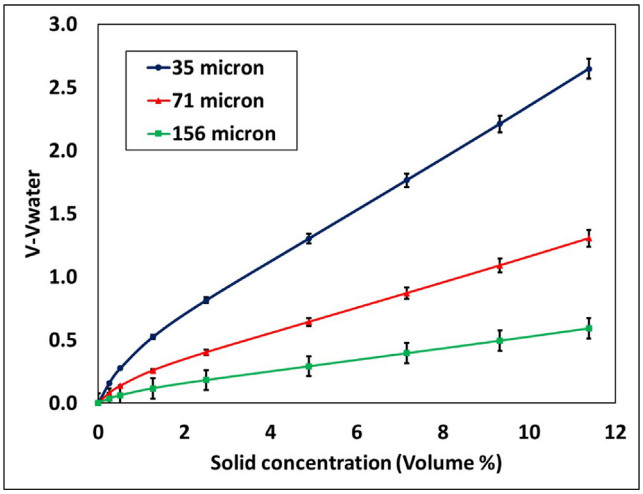

Fig. 2. Calibration curves for various particles.

(MicroBrook particle size analyzer- EyeTech) was applied to define each sample's particle size distribution. It was observed that there was no segregation in the system adopting the particles, which are mentioned in Table 1. In other words, the particle size distribution was independent of the position in the system. So, the OFP can be utilized to measure the solids concentration in the slurry bubble column.

3. Experimental results and discussion

As already mentioned, the solids and gas holdups were measured by the OFPs. In addition, the pressure fluctuations obtained by APT were interpreted to investigate the behaviour of bubbles. The experiments were done at different solid loadings and particle sizes in a wide range of superficial gas velocities. The experiments were carried out at ambient pressure and temperature. For each data point, three experiments were done in order to confirm the accuracy and repeatability of the results. Also, in each run of the experiment, signals were recorded for 180 s. Then, the phase holdups were calculated by the time-average of the data to diminish the effect of the system's non-stationary behaviour on the results. Also, a low pass filter with the cut-off value equal to 60 Hz was used to remove the undesirable digital noises from the recorded signals. It should be mentioned that the frequencies of pressure fluctuations and OFP signals, which are related to the bubbles, are less than the selected cut-off (Esmaeili et al., 2015). The average uncertainty of the gas holdups and solids concentrations, in various positions of the column, were nine and six percent, respectively.

3.1. Pressure fluctuations

Fig. 3 shows the solids loading effect on the standard deviation ratio (SDR) of the pressure fluctuations for 35-μm particles. As is obvious, in the heterogeneous regime (high gas velocities), the SDR increases by the solids loading and superficial gas velocity. This increment due to solids is apparent for 5% solid loading but

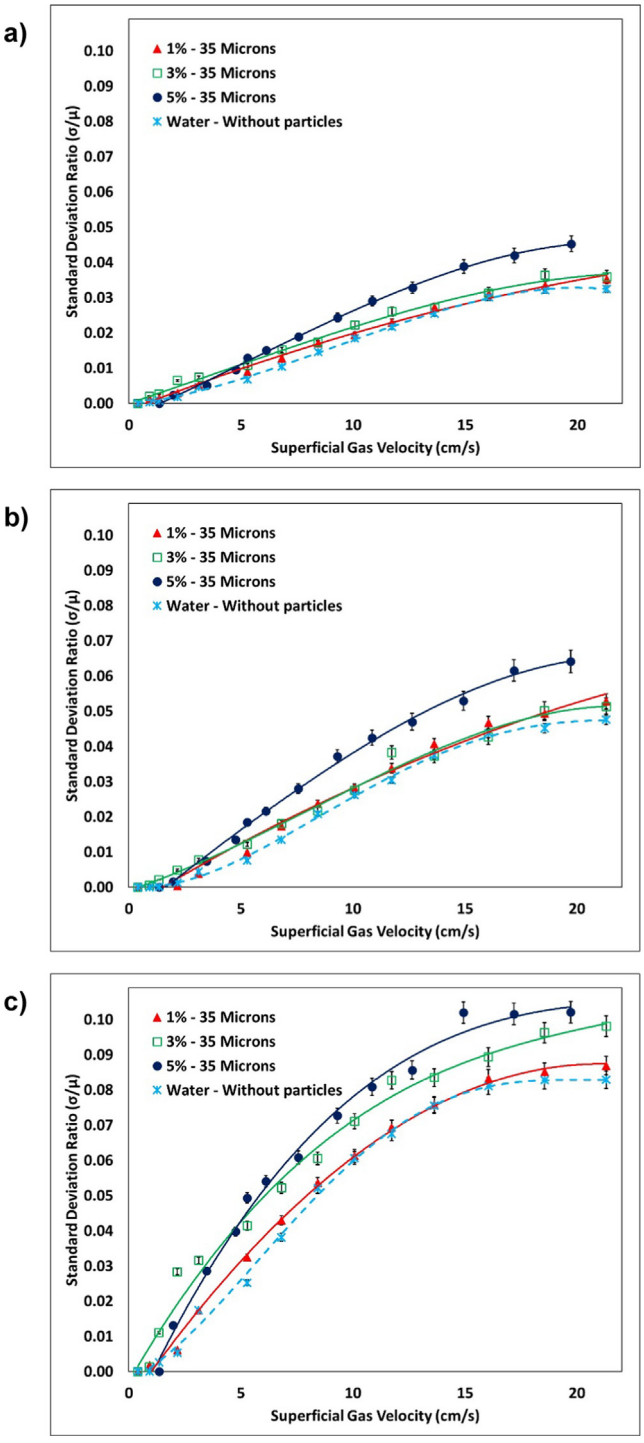

Fig. 3. SD of pressure at various solid loading (a) Bottom (b) Middle (c) Top of the column.

negligible for 1% solids loading. In addition, a clear trend cannot be observed in the homogeneous flow regime, as a noticeable amount of solids cannot be suspended, which may lead to inconsis-

Table 1
Properties of the glass beads particles.

Mean Diameter	Density (kg/m^3)	10% finer than	10% coarser than	Interaction with water
35 μm	2595	18 μm	60 μm	Hydrophilic
71 μm	2595	59 μm	85 μm	Hydrophilic
156 μm	2595	125 μm	192 μm	Hydrophilic

tency in the results. The low amount of the solids has little effect on the initial bubble size, so the SDR does not change at the bottom compared to water. However, the particles' presence leads to an increase in bubble coalescence and, consequently, bubble size. So, it is observed that SDR at the top of the column is more than the bottom. In 5% solids loading, both the initial bubble size and bubble coalescence are highly affected by the presence of the solids. In this case, SDRs are much greater than for water in all positions of the column. It means that the bubble size increased due to the presence of hydrophilic particles. Similar trends were observed for 71 and 156-μm particles.

Fig. 4 shows the effect of the particle size on the SDRs of pressure fluctuations in 5% solids concentration. As expected, the presence of particles with different sizes raises the SDRs in all positions of the column in both homogeneous and heterogeneous regimes. However, a noticeable influence of the particle size on the bubble behaviour can be observed. The amount of SDRs at the bottom of the column is not affected by the particle size, which means that the initial bubble size is independent of the particle diameter. This was also observed for other solids concentrations. The initial bubble size is defined by the gas momentum flux, buoyancy, surface tension, drag and inertial force; however, the primary impact can be attributed to the buoyancy and gas–liquid surface tension, which are barely affected by the particle size (Brian and Chen, 1987).

The standard deviations of the pressure fluctuations in the top area are entirely different for each particle size. It was observed that the SDRs decreased with an increase in the particle diameter. The rate of bubble coalescence is negatively affected by the size of solid particles. This observation is compatible with the results of Sarhan et al. (Sarhana et al., 2018). An increase in particle size results in a reduction in the slurry's apparent viscosity (Senapati et al., 2009); hence, the coalescence rate is negatively affected. Moreover, the large particles' collision induces a higher external force on the bubble that can reduce the large bubble's stability and consequently increase the bubble breakup rate.

3.2. Effect of the superficial gas velocity on the gas and solids holdups

Fig. 5 shows the variation of the local gas holdup by superficial gas velocity. As expected, the gas holdup increases by gas velocity in both the center and near-wall zones. A variation in the gas holdup slope is detected between 2 and 5 cm/s in all cases. This indicates that the transition from the homogeneous to heterogeneous regime occurred in the mentioned range. The transition velocity was not noticeably affected by the particle size. In general, the hydrophilic particles lead to a decrease in the gas holdup (Gheni et al., 2016; Mokhtari and Chaouki, 2019; Orvalho et al., 2018; Lakhdissi et al., 2020). Fig. 5 shows that the amount of gas holdup is highly affected by particle sizes. The decrement of the gas holdup for the small particles is more than that of the large particles. As shown in section 3.1, the small particles lead to the enhancement of bubble coalescence and, consequently, bubble size. The large bubbles tend to escape the system faster than the small bubbles. So, the gas holdup decreases by the increment of the bubble coalescence.

In addition, the gas holdup in the center is higher in comparison to the near-wall (r/R = 0.8) zone. This difference is more apparent at the top of the column due to the tendency of the large bubbles to pass from the centerline of the column. The gas holdup variation from the center to the wall is very high when small particles are used because the creation of large bubbles is augmented by small particles (section 3.1) and the intrinsic behaviour of these bubbles creates a non-uniform radial distribution for the gas holdup. In the sparger zone, the gas holdup distribution mainly depends on the distributor's performance and the flow pattern near the sparger.

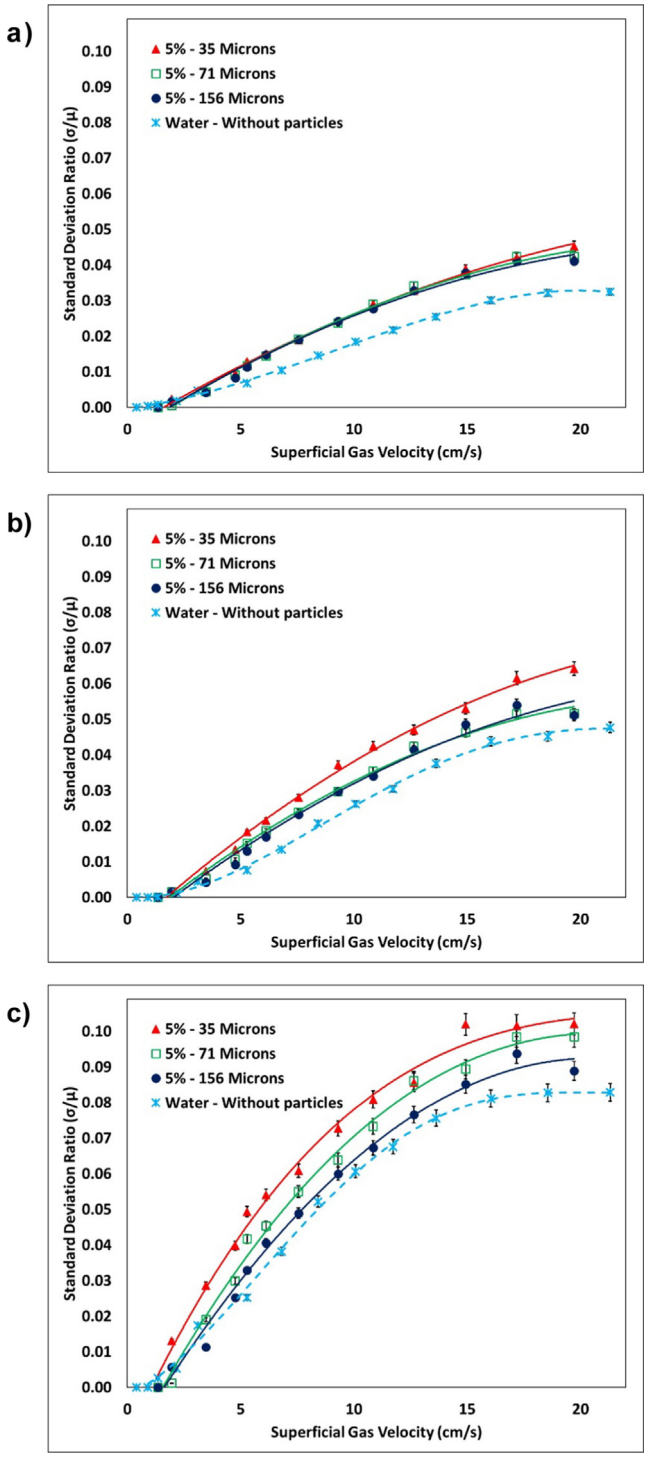

Fig. 4. SD of pressure for various Particle size (a) Bottom (b) Middle (c) Top of the column.

Therefore, the near-wall and centerline gas holdup differences are low compared to the top region.

Fig. 6 shows the dependency of the local solids concentration on the superficial gas velocity for 5% solids loading. The local solids concentration is not uniform, even for small particles. The solids concentration increases by gas velocity as more bubbles have more capability for solids suspension; however, the system can not be well-mixed even at high gas velocities. Although the solids concentration of small particles reaches a plateau at high gas velocities,

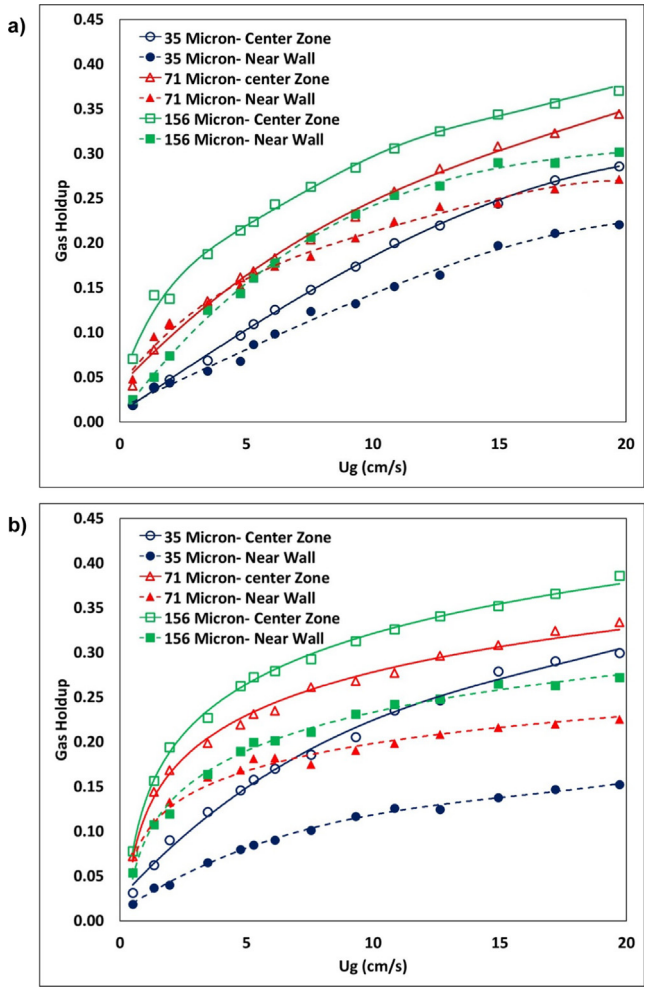

Fig. 5. Gas holdup at various superficial gas velocities at 5% solid loading a) Sparger Zone b) Top of the column.

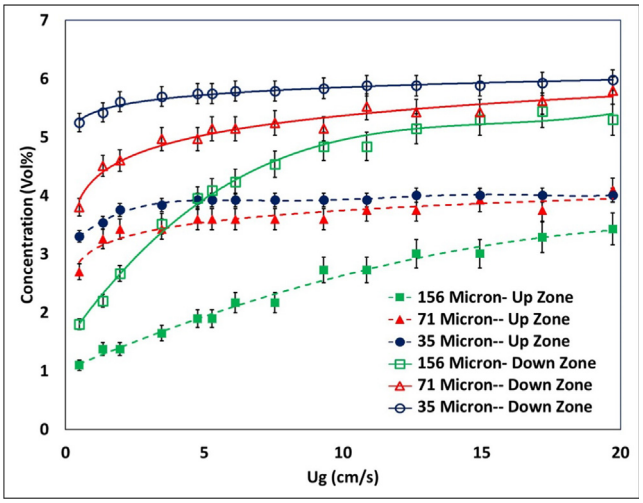

Fig. 6. Variation of the Solid concentration by superficial gas velocity (5% solid loading, r = 0).

the concentration changes depending on the position. It was also observed that the large particles need more gas velocity to reach a constant value due to their higher terminal velocity and the difficulty of the large particle suspension. The difference between the solids concentrations of the bottom and top are considerable, even for small particles.

3.3. Axial distribution of solid particles

Fig. 7 shows the axial distribution of the solid particles for both homogeneous and heterogeneous flow regimes. The concentration of the solids decreases along the axial direction; however, the small particles' concentration shows an increase at the top of the column in the centerline. This happened because of the variation of radial solids distribution along the axial direction, which is discussed in section 3.4. The same trend was reported by the authors elsewhere (Mokhtari and Chaouki, 2019). The difference in the local solids concentration between the bottom and top of the column is noticeable, especially for the homogeneous regime and large particles. The variations are lower for small particles because these particles can easily follow the liquid streamline and suspend along the column. The concentrations are also not uniform radially, as is clear in Fig. 7 for both flow regimes and all particle sizes. The radial variations will be discussed in the following section.

3.4. Radial distribution of phase holdups

Fig. 8 shows the radial distribution of the solid particles for various solid loadings in the column's middle zone. The same behaviours are observed for various solid loadings. The maximum solids concentration is located at the centerline (r = 0), and a local

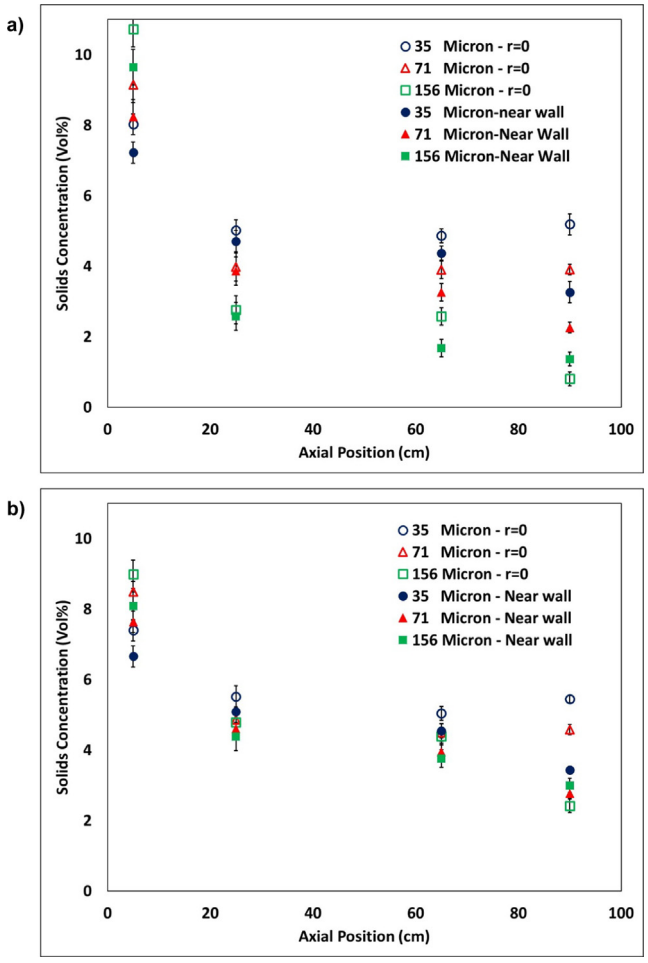

Fig. 7. Axial distribution of Solid Concentration at 5% solid loading a) Homogeneous regime, Ug = 2 cm/s b) Heterogeneous regime, Ug = 15 cm/s.

maximum in concentration appears near r/R = 0.8 in both the homogeneous and heterogeneous flow regimes. Nevertheless, the amount of concentration is lower at the homogeneous flow regime. This local maximum may be attributed to the low liquid velocity in the r/R = 0.7–0.8 in which the axial liquid velocity is near zero and makes it possible for the solid to accumulate. Based on the different correlations in the literature (Wu and Al-Dahhan, 2001), in our column, the zero-velocity of the liquid is in r/R = 0.7–0.8.

Also, the solid particles' radial distribution is more uniform in the homogeneous regime, especially for the small particles. In fact, in the homogeneous regime, liquid macro circulation is weak, and the gas holdup distribution is relatively uniform (Esmaeili et al., 2015); Consequently, the radial variation of the solids concentration is lower than the heterogeneous regime.

It was observed that the trend of the radial solids distribution was roughly independent of the solids loading (in the applied range) because this is mainly a function of the liquid flow pattern and solids properties. Particle size plays an important role in defining the solids distribution. The small particles show higher radial uniformity as they have more capability of following the liquid to form a well-mixed slurry. It should be mentioned that the large particles have a high terminal velocity, which leads to deviation from the liquid streamlines. So, large particles can show stronger radial and axial distribution.

In addition, the trend of the radial solids distribution is changed by height. As shown in Fig. 9a, the solids concentration is nearly uniform in the bottom of the column in all situations because the high shear rate of the sparger makes a well-mixed slurry phase. On the other hand, the solids distribution is entirely different at the top of the column than the sparger zone and the middle zone. Fig. 9b shows that the local maximum in concentration goes to the vicinity of the wall, which could have happened due to the different liquid flow patterns at the top, but more investigation is required to define the reason for this phenomenon. Fig. 9b also depicts that large particles (156 μm) have a very low concentration in the centerline (r = 0). It seems that the bubbles do not have enough energy to uplift these particles into the top zone. Also,

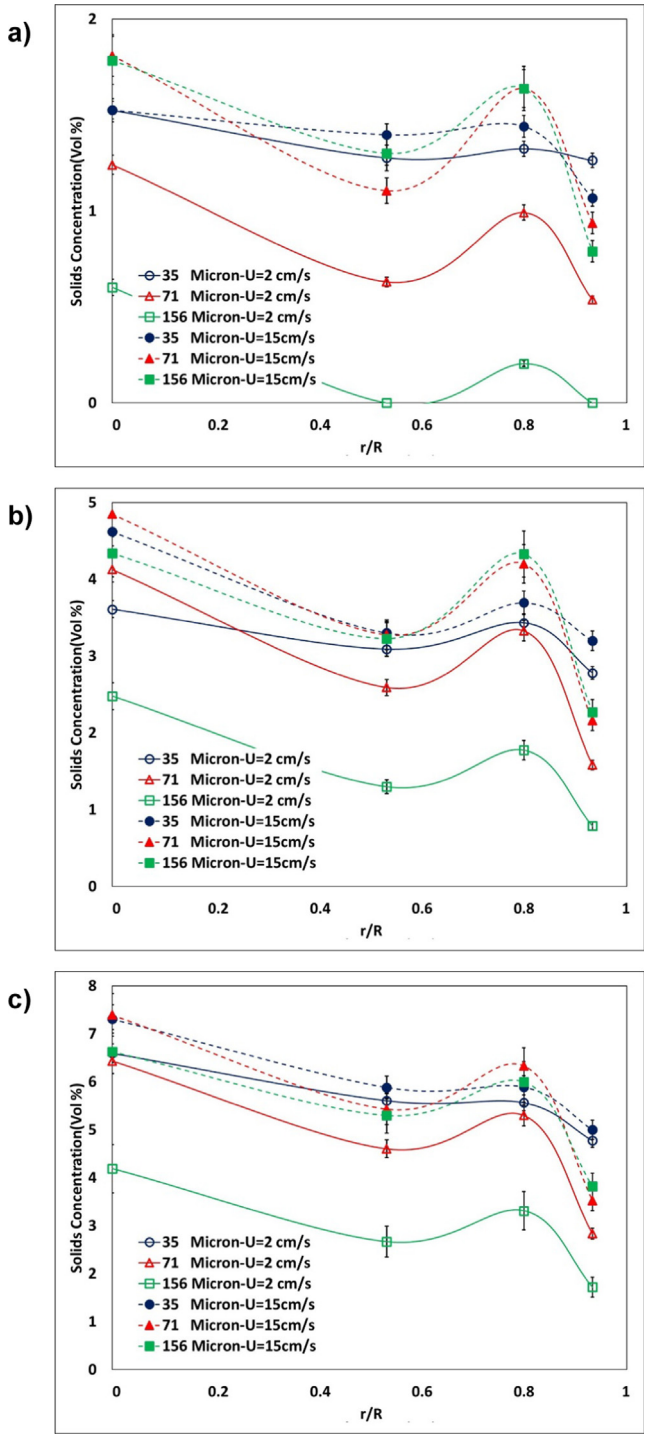

Fig. 8. Radial distribution of the solid concentration Middle zone a) 1% solid loading b) 3% solid loading c) 5% solid loading.

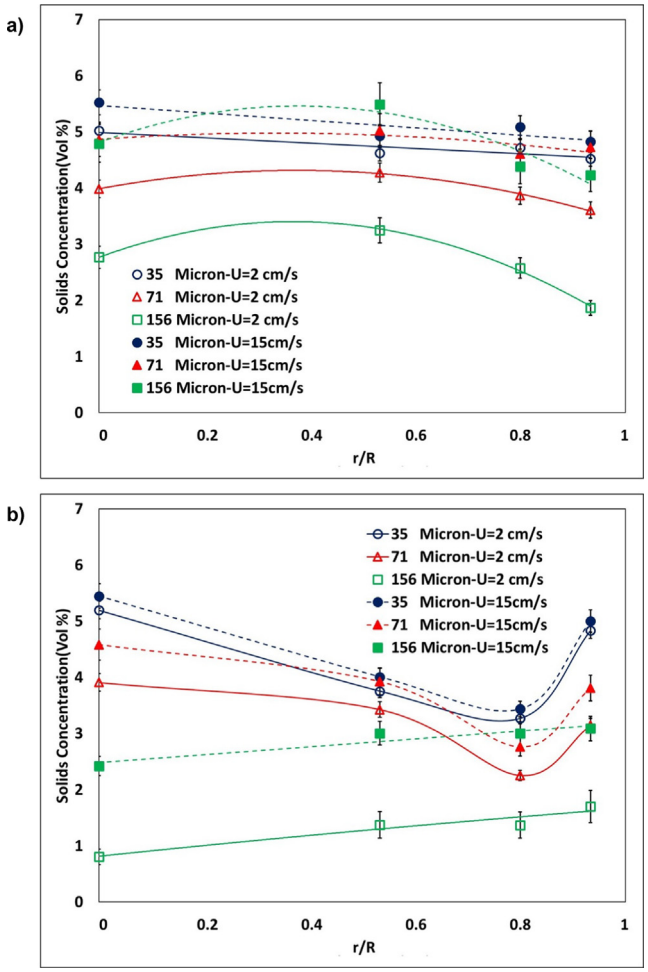

Fig. 9. Radial Distribution of the solid concentration at 5% solid loading a) Sparger Zone b) Top of the column.

the presence of the large particles deviates the bubbles from the centerline to the near-wall area. So, there are not enough bubbles in the center to lift the particles.

This bubble deviation is apparent in Fig. 10, which shows the gas holdup's radial variation in the middle and top area of the column for both homogeneous and heterogeneous flow regimes. The maximum gas holdup occurs at the center (r = 0) except for the 156-μm particles. These large particles can change the direction of the bubbles due to their high momentum. As shown in Fig. 8, the particles' concentration at the center is high, which can hinder the bubbles, especially at high solid loading. The gas holdup in the center is thus diminished, and the maximum holdup falls in the radius near r/R = 0.5 where the solids concentration is low.

Based on the achieved results, in general, an increase in concentration and a decrease in the particle size led to a decrease in the gas holdup. As already discussed, the hydrophilic solids reduce the gas holdup because of the bubble size's enlargement. It was observed that the small particles had more influence on bubble coalescence (Section 3.1). Thus, the reduction in gas holdup was more substantial for small particles.

Fig. 10 depicts a remarkable difference between the homogeneous and heterogeneous flow regimes. The increment in the solids concentration caused an enhancement in the gas holdup for low superficial gas velocity (Fig. 10 a, b). This phenomenon can be attributed to the low interaction between bubbles in the homogeneous flow regime. The coalescence rate was negligible at low gas velocity, and the increase in solids concentration means an increase in the force acting against the bubbles' movement. So, the increase in the solid loading reduced the bubble rise velocity and consequently increased the gas holdup. In contrast, in the heterogeneous flow regime (Fig. 10c, d), the bubble coalescence dominated the system, and therefore, an increase in the solids loading, which enhances the bubble coalescence, could decrease the gas holdup.

4. Modeling

The distribution of solid particles, as catalyst or reactant, greatly affects the reactor's performance. A well-mixed assumption may lead to significant errors in the design of reactors. Predictive models should therefore be used to increase the quality of the SBCR's design and scale-up. Some researchers (Abdullah, 2019; Reilly et al., 1990; Cova, 1996; Kato et al., 1972) tried to develop models to predict the solids distribution in slurry bubble columns, but they all assumed that the radial solids concentration is uniform. In section 3, it was observed that the solids concentration varied in the radial direction. Consequently, a predictive model should consider both radial and axial solids distribution. In the present study, a two dimensional (r,z) model was developed.

The movement of solid particles in a liquid inside a bubble column reactor may be investigated by considering various parameters. The liquid flow pattern has the main influence on the motion of the solids; however, solid particles show a downward movement due to gravity. This falling velocity is highly affected by the particle size and shape, as well as liquid density, solid density, and liquid viscosity.

The variations along θ in (r, z, θ) coordinates were neglected. It was also assumed that the column was in a steady state, which means the radial and axial solids distribution remain constant in time. Also, the variation of the gas holdup along the z-direction was neglected.

The mass balance for the solid phase for a tiny element of the bed, as shown in Fig. 11, is as follows.

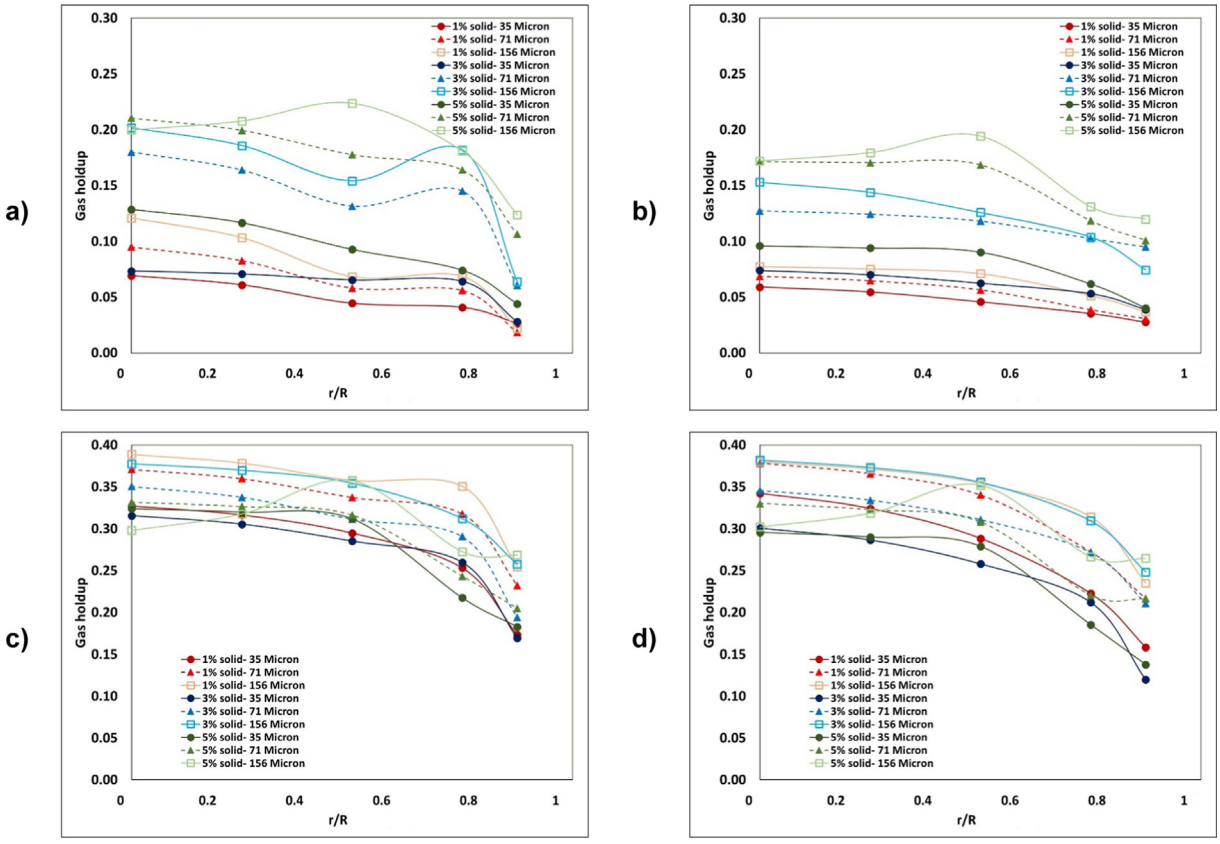

Fig. 10. Radial Gas holdup at various solid loadings and particle sizes a) Homogeneous, Middle zone b) Homogeneous, Top zone c) Heterogeneous, Middle zone d) Heterogeneous, Top zone.

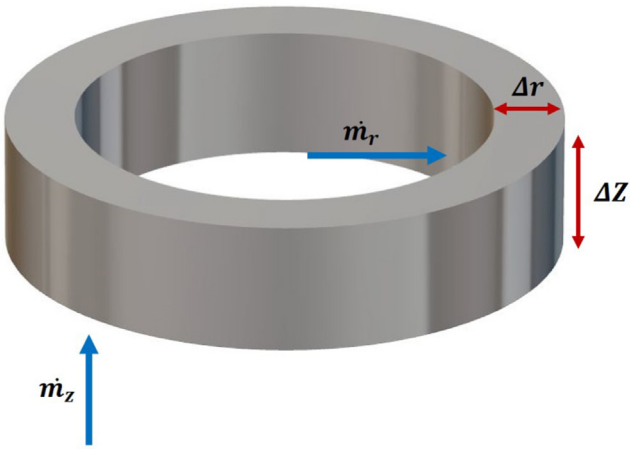

Fig. 11. Small element of the bed for mass balance.

$$\dot{m}_z(2\pi r\Delta r)(1-\varepsilon_g)|_z - \dot{m}_z(2\pi r\Delta r)(1-\varepsilon_g)|_{z+\Delta z}\cdots$$

$$\cdots + \dot{m}_r(2\pi r\Delta z)(1-\varepsilon_g)|_r - \dot{m}_r(2\pi r\Delta z)(1-\varepsilon_g)|_{r+\Delta r} = 0 \quad (1)$$

In which, the $\dot{m}_z$ and $\dot{m}_r$ are the axial and radial mass flux of the particles, and can be described as,

$$\dot{m}_z = V_{SL}.C - V_p.C - D_s\frac{\partial C}{\partial z} \quad (2)$$

$$\dot{m}_r = -D_s\frac{\partial C}{\partial r} \quad (3)$$

The velocity profile of the slurry phase, V_{SL}, is defined by (Wu and Al-Dahhan, 2001);

$$V_{SL} = V_0\left(1 - 2^{N/2}\left(\frac{r}{R}\right)^N\right) \quad (4)$$

The liquid velocity in the radial direction is neglected; however, the axial liquid velocity has a radial profile as shown in Eq. (4). The V_p , in Eq. (2), is the deviation of the particle velocity from the liquid velocity which is called slip velocity. Also, the D_s is the dispersion coefficient of the solid particles.

Eq. (1) should be written in the differential form, so for a very small Δr and Δz, the equation can be written as a partial differential equation.

$$(1-\varepsilon_g)\frac{\partial \dot{m}_z}{\partial z} + \frac{1}{r}\frac{\partial}{\partial r}\left[(1-\varepsilon_g)\dot{m}_r.r\right] = 0 \quad (5)$$

And by substituting the $\dot{m}_z$ and $\dot{m}_r$ from Eqs. (2) and (3) into the Eq. (5), the PDE is,

$$(1-\varepsilon_g)\frac{\partial}{\partial z}\left[(V_{SL}-V_p)C - D_s\frac{\partial C}{\partial z}\right] + \frac{D_s}{r}\frac{\partial}{\partial r}\left[(1-\varepsilon_g)\frac{\partial C}{\partial r}.r\right] = 0 \quad (6)$$

Also, the gas holdup in Eq. (6) is a function of r. This radial functionality made the PDE more complicated. The following equation is proposed to estimate the radial distribution of the gas holdup (Wu et al., 2001).

$$\varepsilon_g = \varepsilon_g\frac{n+2}{n}\left[1 - 0.5\left(\frac{r}{R}\right)^n\right] \quad (7)$$

In which, ε_g is the overall gas holdup inside the column and n is a constant depending on the process situation.

The separation of variables technique was used to solve the PDE, after substituting the Eq. (7) into

Eq. (6). Also, the following boundary conditions were applied.

$$r = 0 \rightarrow \frac{\partial C}{\partial r} = 0$$

$$z \rightarrow \infty \rightarrow c = 0$$

$$\frac{\int_0^{2\pi}\int_0^r\int_0^L c(r,z).r.dzdrd\theta}{\pi R^2 L} = C_0$$

The symmetry boundary was applied at the centerline. Also, the solids concentration becomes zero at the infinite height if the density of the solids is more than that of liquid. The third condition indicates the fact that the volume average of solids concentration is equal to C_0. Here, L is the bed height and can be obtained by $L = \frac{L_0}{\varepsilon_g}$, and the C_0 is the overall solids concentration in the slurry.

Finally, the following equation is obtained by the PDE's analytical solution, capable of estimating the radial and axial solids distribution inside the SBCRs.

$$C(r,z) = K.exp(-Pe_z).\left(1 - \frac{{Pe_R}^2}{4\xi}\frac{r^2}{R^2}\right) \quad (8)$$

$$k = C_0\frac{Pe_L}{\left[\frac{{Pe_R}^2}{8.\xi} - 1\right][\exp(-Pe_L) - 1]} \quad (9)$$

Here, the ξ is the slip ratio which is defined as $\frac{V_p}{V_0}$, and V_0 is the axial slurry velocity in the centerline of the column. Some correlations are available to estimate this velocity (Wu and Al-Dahhan, 2001). In addition, the Peclet numbers are $Pe_z = \frac{V_p.Z}{D_s}$,$Pe_R = \frac{V_p.R}{D_s}$, $Pe_L = \frac{V_p.L}{D_s}$.

The value of V_p and D_s should be defined to be able to use this model. There are some correlations in the literature which can be applied to estimate these values (Reilly et al., 1990; Kato et al., 1972).

$$\frac{V_p}{D_s} = 573\left(\frac{V_t}{\rho_L}\right)^{2/3}.\left[\frac{\rho_S - \rho_L}{\rho_L}\right]^{1/3}{U_G}^{-0.1} \quad (10)$$

$$V_p = 1.33V_t(U_G/V_t)^{0.25}(1-C_V)^{2.5} \quad (11)$$

Experimental data of the present study and literature (Warsito et al., 1999; Soong et al., 2000; Rados et al., 2005; Reilly et al., 1990) were adopted to examine the developed model's accuracy. Fig. 12 shows that the present model can provide a reasonable prediction for the solids concentration in various particle sizes with different solids loading. As depicted in this figure, the radial variation increases with the particle size and solid loading. The model predicts these effects properly. The model is not capable of predicting the near-wall peak, which was already discussed in section 3. In addition, the model is not applicable at both ends of the column, because in these zones, the liquid flow pattern and the gas holdup distribution are entirely dissimilar to what was assumed in the model. However, it generally provides a satisfactory estimation in the zone away from the sparger and top.

Fig. 13 displays the comparison of the experimental data with the values that have been predicted by the present model in both axial and radial directions. The mean absolute percentage error (MAPE) was 18.5%. The MAPE is calculated based on over 400 data points from the present study and the literature (Warsito et al., 1999; Soong et al., 2000; Rados et al., 2005; Reilly et al., 1990). It should be noted that the experimental data cover various particle sizes, column sizes, and process situations, which proves the reliability of the model in different conditions.

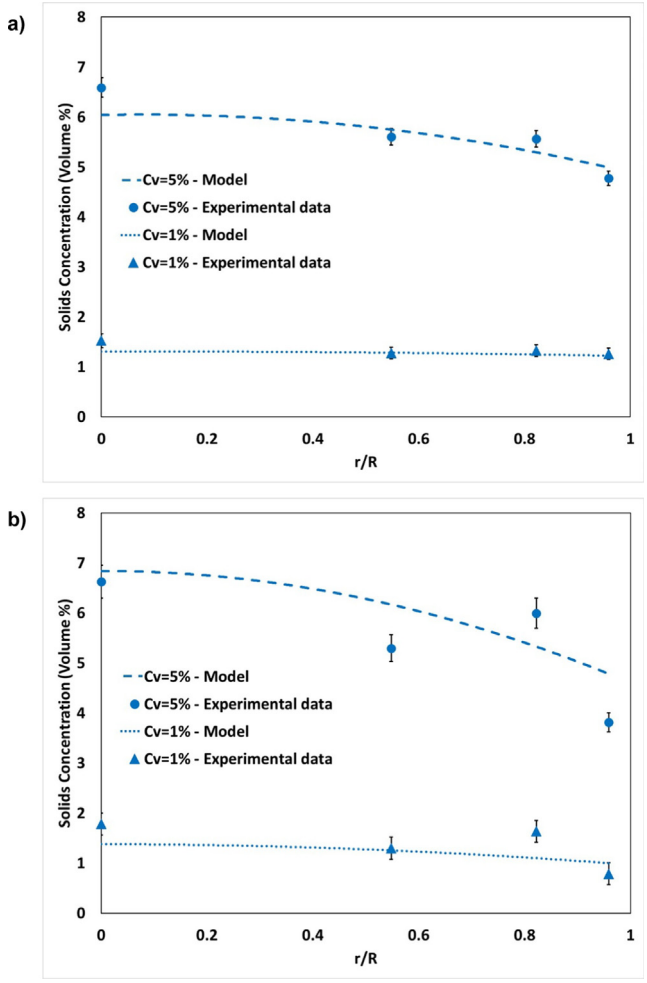

Fig. 12. Prediction of the solid concentration at the middle of column by the present model a) 35 μm b) 156 μm mean particle diameter.

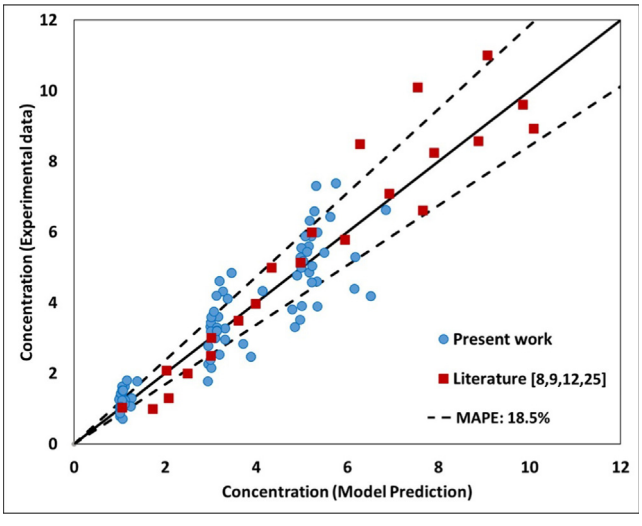

Fig. 13. Model versus experimental data.

5. Conclusion

In this study, the effects of particle size and concentration on the local hydrodynamics of the SBCRs were investigated by using optical fiber probes and absolute pressure transducers. A new method already presented by the authors (Mokhtari and Chaouki, 2019) was adopted for the simultaneous measuring of solids and gas holdup in the slurry bubble column.

It was observed that the radial and axial phase holdup distributions were not uniform in the slurry bubble column. Also, different particle sizes showed distinct behaviors. The obtained results can be summarized as follows,

- The pressure fluctuations showed that the small particles led to more bubble coalescence, but the initial bubble size was independent of the particle size.
- The presence of hydrophilic particles led to a reduction in the gas holdup. This reduction was more evident in smaller particles.
- A local maximum for radial solids concentration was observed in the near-wall region in the middle of the column.
- The radial solids concentrations were fairly uniform in the sparger zone.
- The particle size did not have a remarkable influence on the shape of radial solids distribution; however, the amount of concentration, specially at the top, was low for large particles due to the difficulty in the suspension.
- Gas holdup showed a parabolic radial distribution except for large particles at high solids loading.
- The phenomenological model could properly predict the spatial solids distribution in the SBCRs at various conditions.

CRediT authorship contribution statement

Mojtaba Mokhtari: Methodology, Investigation, Writing - review & editing. **Jamal Chaouki:** Supervision, Writing - review & editing.

Declaration of Competing Interest

The authors declare that they have no known competing financial interests or personal relationships that could have appeared to influence the work reported in this paper.

Acknowledgements

The authors would like to thank the TOTAL American Services, Inc. and the Natural Science and Engineering Research Council, Canada (NSERC) for their financial support of this study.

References

Abdullah, H.M., 2019. Study of Axial Solid Concentration Distribution in Slurry Bubble Columns. Energy Procedia. 157, 1537–1545.
An, M., Guan, X., Yang, N., 2020. Modeling the effects of solid particles in CFD-PBM simulation of slurry bubble columns. Chem. Eng. Sci. 223, 115743.
Besagni, G., Inzoli, F., 2016. Comprehensive experimental investigation of counter-current bubble column hydrodynamics: Holdup, flow regime transition, bubble size distributions and local flow properties. Chem. Eng. Sci. 146, 259–290.
Brian, B.W., Chen, J.C., 1987. Surface tension of solid-liquid slurries. AIChE J. 33, 316–318.
Cova, D.R., 1996. Catalyst suspension in gas-agitated tubular reactors. Ind. Eng. Chem. Process Des. Devel. 5, 20–25.
Esmaeili, A., Guy, C., Chaouki, J., 2015. Local Hydrodynamic Parameters of Bubble Column Reactors Operating with Non-Newtonian Liquids: Experiments and Models Development. AIChE J. 62, 1382–1396.
Esmaeili, A., Guy, C., Chaouki, J., 2015. The effects of liquid phase rheology on the hydrodynamics of a gas–liquid bubble column reactor. Chem. Eng. Sci. 129, 193–207.
Gheni, S.A., Abdulaziz, Y.I., Al-Dahhan, M.H., 2016. Effect of L/D Ratio on Phase Holdup and Bubble Dynamics in Slurry Bubble Column using Optical Fiber Probe Measurements. Int. J. Chem. React. Eng. 14, 653–664.
Hernandez-Alvarado, F., Kleinbart, S., Kalaga, D.V., Banerjee, S., Joshi, J.B., Kawaji, M., 2018. Comparison of void fraction measurements using different techniques in two-phase flow bubble column reactors. Int. J. Multiphase Flow. 102, 119–129.

Jin, H., Han, Y., Yang, S., He, G., 2010. Electrical resistance tomography coupled with differential pressure measurement to determine phase hold-ups in gas-liquid-solid outer loop bubble column. Flow. Meas. Instrum. 21, 228–232.
Kato, Y., Nishiwaki, A., Fukuda, T., Tanaka, S., 1972. The behavior of suspended solid particles and liquid in bubble columns. J. Chem. Eng. Japan. 5.
Kim, Y.H., Tsutsuni, A., Yoshida, K., 1987. Effect of particle size on gas holdup in three-phase reactors. Sadhana 10, 261–268.
Lakhdissi, E.M., Soleimani, I., Guy, C., Chaouki, J., 2020. Simultaneous effect of particle size and solid concentration on the hydrodynamics of slurry bubble column reactors. AICHE J. 66.
Manjrekar, O.N., Dudukovic, M.P., 2015. Application of a 4-point optical probe to a Slurry Bubble Column Reactor. Chem. Eng. Sci. 131, 313–322.
Mokhtari, M., Chaouki, J., 2019. New technique for simultaneous measurement of the local solid and gas holdup by using optical fiber probes in the slurry bubble column. Chem. Eng. J. 358, 831–841.
Orvalho, S., Hashida, M., Zednikova, M., Stanovsky, P., Ruzicka, M.C., Sasaki, S., Tomiyama, A., 2018. Flow regimes in slurry bubble column: Effect of column height and particle concentration. Chem. Eng. J. 351, 799–815.
Prakash, B., Parmar, H., Shah, M.T., Pareek, V.K., Anthony, L., Utikar, R.P., 2019. Simultaneous measurements of two phases using an optical probe. Exp. Comput. Multiphase Flow. 1, 233–241.
Rabha, S., Schubert, M., Hampel, U., 2013. Intrinsic flow behavior in a slurry bubble column: A study on the effect of particle size. Chem. Eng. Sci. 93, 401–411.
Rados, N., Shaikh, A., Al-Dahhan, M., 2005. Phase Distribution in a High Pressure Slurry Bubble Column via a Single Source Computed Tomography. Can. J. Chem. Eng. 83.
Reilly, I.G., Scott, D.S., de Bruijn, T.J.W., MacIntyre, D., Piskorz, J., 1990. Axial solids concentrations in three-phase bubble columns. Chem. Eng. Sci. 45, 2293–2299.
Ruthiya, K.C., Chilekar, V.P., Warnier, M.J.F., van der Schaaf, J., Kuster, B.F.M., Schouten, J.C., van Ommen, J.R., 2005. Detecting regime transitions in slurry bubble columns using pressure time series. AIChE J. 51, 1951–1965.
Sarhana, A.R., Nasera, J., Brooks, G., 2018. Effects of particle size and concentration on bubble coalescence and froth formation in a slurry bubble column. Particology. 36, 82–95.
Senapati, P.K., Panda, D., Parida, A., 2009. Predicting Viscosity of Limestone-Water Slurry. J. Minerals. Mat. Characteriz. Eng. 8, 203–221.
Shu, S., Vidal, D., Bertrand, F., Chaouki, J., 2019. Multiscale multiphase phenomena in bubble column reactors: A review. Renew. Energy. 141, 613–631.
Sines, J.N., Hwang, S., Marashdeh, Q.M., Tong, A., Wang, D., He, P., Straiton, B.J., Zuccarelli, C.E., Fan, L.S., 2019. Slurry bubble column measurements using advanced electrical capacitance volume tomography sensors. Powder Technol. 355, 474–480.
Soong, Y., Fauth, D.J., Knoer, J.P., 2000. Ultrasonic characterizations of solids holdup in a bubble column reactor. Chem. Eng. Technol. 23, 751–753.
Wang, F., Jin, N.D., Wang, D.Y., Han, Y.F., Liu, D.Y., 2017. Measurement of gas phase characteristics in bubbly oil-gas-water flows using bi-optical fiber and high-resolution conductance probes. Exp. Therm. Fluid. Sci. 88, 361–375.
Warsito, M., Ohkawa, N., Kawata, S., 1999. Uchida, Cross-sectional distributions of gas and solid holdups in slurry bubble column investigated by ultrasonic computed tomography. Chem. Eng. Sci. 54, 4711–4728.
Wu, Y., Al-Dahhan, M., 2001. Prediction of axial liquid velocity profile in bubble columns. Chem. Eng. Sci. 56, 1127–1130.
Wu, Y., Ong, B.C., Al-Dahhan, M., 2001. Predictions of radial gas holdup profiles in bubble column reactors. Chem. Eng. Sci. 56, 1207–1210.
Zhou, R., Yanga, N., Li, J., 2020. A conceptual model for analyzing particle effects on gas-liquid flows in slurry bubble columns. Powder Technology. 365, 28–38.